International Journal of Current Trends in Engineering & Research (IJCTER)
e-ISSN 2455–1392 Volume 2 Issue 2, February 2016 pp. 59 - 67
Scientific Journal Impact Factor : 3.468
http://www.ijcter.com

Analysis of Fatigue Due to Thermal Stress in Induction Rotor

Mohd. Shakib Hussain[1]

[1]*Department of Mechanical Engineering*

Abstract—The electromagnetic behavior of the induction rotor is obtained by coupling the field equations to the voltage equations of the windings. The nonlinearity due to the saturation of the iron core and the temperature dependency of the electrical conductivity are taken into account, since it leads to thermal stress. When the heat sources are evaluated the temperature distribution in the induction motor is obtained. In order to improve the accuracy of the formulation, thermal contact resistances, external and internal convection are considered. This paper analyzes the thermal stresses on the rotor of an induction motor and performance of rotor in terms of fatigue. The mechanical deformations and thermal stress distributions are obtained. The numerical analyzes of the thermal field are verified by various experimental results. The results presented in this paper prove that the thermal stress of electric material characteristics must be considered, to accurately prove the fatigue behavior of the induction rotors during the design stage.

Keywords—Iron Core, Dynamic Modeling, induction rotor, torque, fatigue, contact resistances, etc.

I. INTRODUCTION

The common electrical motor utilized as a part of mainly applications which is known as Induction motor. The synchronous speed will runs more at a speed in this motor then it is called as asynchronous motor. The rotating machine gives the speed of revolution of the magnetic field and number poles of the machine and it relies on the frequency. An Induction motor dependably keeps running at a speed not exactly synchronous speed due to the rotating magnetic field which is generated in the stator which will formulate the rotor to revolve then it will produce flux in the rotor, however, since flux current in the stator will lag the flux current in the rotor, the rotor will never attain to its rotating magnetic field speed such as the synchronous speed. There are essentially two sorts of induction motor that rely on the input supply.

II. RELATED WORK

Researchers surveyed about compound cage rotor having 3kW two poles induction motor. Initially, at various loads the temperature distribution of rotor is premeditated then, the outcome of temperature field is taken into computation of thermal stress field [1]. Computation is:

- The load will increase when maximum thermal stress is amplified.
- In between the lower cast aluminum and upper compound material it has some mutual extruding. Particularly, at the sharp corners of border of two types of material, the thermal stress is maximum

They showed that accuracy can be explicated by the factors area as follows: accurate calculation of aggregate inertia constant, precise computation of equivalent-circuit impedances and sufficient conduct with load power-slip characteristics of individual motors. Alternatively, the computational exertion needed in edifice the aggregate model is not profound. Additionally, double-cage rotors can be expanded without any obstructions. The aggregation method can extensively be applied to large efficacy power networks for constituting load characteristics in addition to large industrial power systems for the period of simulation reports of dynamic Transients [2].

III. THEORETICAL DEVELOPMENT

A. Structure of 2D temperature field model

The 2-D temperature field model can be used in induction motor for eg., compound cage motor which is shown in Figure 3.1. For changing the model, it will take some theories. They are as:[3]:

- The heat flux in the axial direction of rotor is zero.
- The cooling fin measures the disseminating heat cause of base around.
- There is on heat relocate between shaft and rotor core.

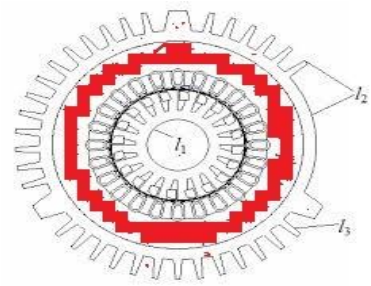

Figure 3.1.Thermal analysis of induction motor with compound cage motor [34].

B. Temperature distribution of rotor of induction motor

The lowest temperature bar and the highest temperature bar are taken for aim of the study. The temperature allotment in single bar is progressively decreased from the top to the bottom of the bar and the lowest temperature at the top of the bar. These temperature differences are lower than 0.5°C. The temperature division of bar has the highest temperature at the rated load.

C. Structure of 2D-thermal stress model

A thermal stress of each node is solved though the outcome of temperature field is loaded to thermal stress field. The issue of elastic distortion in mechanical system can be examined by the relationship between strain potential energy and transformation depends upon the lowest potential energy of system.

$$\Pi = U + \Omega \tag{3.1}$$

Where, Π is the total potential energy; U is the strain potential energy of internal system; Ω is the system potential energy found by external force.

The deformation of rotor is distant lower than the geometric size of itself can be used for the evaluation of thermal stress in rotor. Consequently, higher order is disregarded and examining by finite element. Equation (3.7) can be interpreted into:

$$\left(\sum_1^n \int_s B^T DBdS \right).\delta = \sum_1^n \int_s B^T D\varepsilon_0 dS \tag{3.2}$$

Where B is unit stress matrix; D is the elastic coefficient matrix;
δ is the system displacement vector; ε_0 is the unit thermal stress matrix;
n is unit number.

If α_x, α_y indicate thermal development coefficient of x, y direction correspondingly and Δt imply temperature increase, then ε_0 can be meant that:

$$\varepsilon_0 = \left[\alpha_x \Delta t, \alpha_y \Delta t, 0, 0 \right]^T \tag{3.3}$$

D. Evaluation of iron loss in induction motor

The tangential and normal components of the flux density were calculated in the separated elementary regions of a 2D FEM. These regions can be randomly petite, thus the flux density are steady in the region by considering the both possible components. The FEM model can be used to calculate the results; it is stored and utilized in post processing mode, and where in all elementary regions the iron loss components can be calculated. In evaluating method of iron loss components, it was implicit that the iron loss below revolving field is the total of the iron loss below irregular conditions in tangential (Θ) and radial (r) directions. The effect of revolving magnetic field can be considered by the static hysteresis loss P_h and can be computed by the following equation,

$$P_h = \frac{1}{T}\sum_{i=1}^{N}(B_{mri}^{\alpha} + B_{m\Theta i}^{\alpha}).k_{hi}^{*} \qquad (3.4)$$

where

k_{hi}^{*} is the coefficient based on material parameters and elementary volume of the B vector loci in *i*th region with ellipticity,

α is the hysteresis loss coefficient,

B_{mri}^{α}, $B_{m\Theta i}^{\alpha}$ are the highest value of the tangential and normal component of the flux density in *i*th region,

N is the number of regions and T is the fundamental harmonic period.

As a result, the solution to the issue based on the hypotheses, established by various researchers, that lacking minor loops, the static hysteresis loss based only on the peak of flux density. The issue is more complex in the case of minor loop subsistence. Several researchers recommended utilizing an easy formula and summing up the static hysteresis losses, initiating from high-order and fundamental harmonics [4]. Conversely, the diverse initial phases and the same amplitude of harmonics will vary the highest value of the distorted flux and thus, the overall static hysteresis loss. Furthermore, these can guide to the incident of the minor loops**.**

IV. EXPERIMENTS AND OBSERVATIONS

A. Iron loss model

The computation of iron losses can be attained utilizing the disintegration of the iron losses in three parts are as follows:

$$P_t = P_h + P_{cl} + P_{exc} \qquad (4.1)$$

Where, P_h -hysteresis; P_{cl} -classic eddy-current; and P_{exc} - excess losses. For a non-sinusoidal excitation and taking into account laminations, the (4.1) equation can be as follows:

$$P_t = P_h + k_{cl}\frac{1}{T}\int_0^T\left(\frac{dB(t)}{dt}\right)^2 dt + k_{exc}\frac{1}{T}\int_0^T\left|\frac{dB(t)}{dt}\right|^{1.5} dt \qquad (4.2)$$

Where, T - period of the excitation waveform

dB/d*t* - time derivative of the magnetic flux density and

k_{cl} and k_{exc} - loss coefficients linked to the material properties.

With the calculated data, a curve fitting can be attained and by adding up the iron loss components, the rotor can be achieved. In the rotor and stator hysteresis losses (P_h), three distinct execution methods were tested [5].

1) The initial method calculates the hysteresis losses in every element *i* depends upon the first stator scheduling harmonic frequency (*fs*) where α and k_h are parameters attained from the dimensions.

$$P_h = k_h f_s \sum_{i=1}^{n} B_{m,i,j^*}^{\alpha} \tag{4.3}$$

2) The second method utilizes a Fourier transform and the hysteresis losses are attained from adding up the contribution of every harmonic *j* of the magnetic field

$$P_h = k_h f_s \sum_{i=1}^{n} \sum_{i=1}^{m} f_{i,j} B_{m,i,j^*}^{\alpha} \tag{4.4}$$

3) A third method computes the hysteresis losses utilizing the fundamental frequency (f_f) of the magnetic field connected to every element of the finite-element (FE) mesh, f_f being the harmonic with the highest amplitude,

$$P_h = k_h \sum_{i=1}^{n} f_{f,i} B_{m,i}^{\alpha} \tag{4.5}$$

Due to the dynamic components of equation (4.2) (P_{cl} and P_{exc}) are only suitable for laminated materials, the traditional eddy currents of the solid rotor are calculated by the 2-D FE code and its overload losses are ignored. Hence, once the steady state is achieved, the vector component of the magnetic field manufactures the locus of every FE in the iron. Subsequently, the iron losses with the abovementioned three approaches were calculated by utilizing the minor and major axes. As an initial method, the rotating iron losses of an FE are unspecified to be the amount of iron losses connected to the minor and major axes:

$$P_{t,iron} = \sum_{i=1}^{n} (P_{t,i}^{maj} + P_{t,i}^{\min}) \tag{4.6}$$

B. Field Equations

From magnetic vector potential and Maxwell equations, the field equations are attained are as follows:

$$\begin{cases} \nabla \times (\upsilon \nabla \times A) = 0 \\ \nabla \times (\upsilon \nabla \times A) = J_{ex} \\ \nabla \times (\upsilon \nabla \times A) = 0 \\ \nabla \times (\upsilon \nabla \times A) + j\omega g \sigma_E A + \sigma_E \nabla V = 0 \\ A = 0 \end{cases} \tag{4.7}$$

where, A is the magnetic vector potential,

J_{ex} is the source current density, G is the slip,

υ is the reluctivity, σ_E is the electrical conductivity,

V is the electric scalar potential, υ_s is the pulsation of the source voltage,

The finite element expression of the field equations are as follows:

$$\begin{cases} [S][A] - [P][i_{enc}] = 0 \\ [S][A] = 0 \\ [S][A] + j\omega_s g[G][A] = 0 \\ [S][A] = 0 \end{cases} \tag{4.8}$$

with:

$$\begin{aligned} S_{ij} &= l \iint_{\Omega} \upsilon \nabla N_i \nabla N_j d\Omega \\ P_i &= \frac{l N_{cond}}{S_{Cu}} \iint_{\Omega} N_i d\Omega \\ G_{ij} &= l\sigma \iint_{\Omega} N_i N_j d\Omega \end{aligned} \tag{4.9}$$

$[i_{enc}]$ is the column vector of the current in a stator slot,

L is the length of the stator conductors/length of the core region,

N_{cond} is the number of turns in series in a coil,

S_{Cu} is the cross sectional area of copper in coil side.

C. Voltage equations

The finite element region is superficially associated by the source voltage. The following matrix equation shows the rotor equivalent circuit:

$$[U_i]=[R_{tete}][i_{ph_i}]+j\omega_s[L_{tete}][i_{phi}]+[\Delta V_i], i=1,2,3 \quad (4.10)$$

Where, $[U_i]$ is the external source voltage of the i*th* phase winding?

$[R_{tete}]$ is the end-winding resistance matrix; $[L_{tete}]$ is the end-winding inductance matrix,

$[\Delta V_i]$ is the scalar potential difference induced in the ith phase winding,

$[i_{phi}]$ is the current of the ith phase winding.

By employing Ohm's law on the coil sides of the phases winding, the scalar potential differences caused in the phases of the rotor windings were achieved.

$$\Delta V_{enc}=R_{enc}i_{enc}+j\omega_s\frac{lN_{cond}}{S_{Cu}}\iint_{\Omega}\sum_{i=1}^{n_p}(N_iA_i)d\Omega \quad (4.11)$$

Where, $[R_{enc}]$ is the slot's resistance matrix,

$[\Delta V_{enc}]$ is the column vector of the scalar potential differences induced in the stator slot.

The connection matrix [C] can be acquainted as:

$$\begin{aligned}[i_{enc}]&=[C]^T[i_{ph}]\\ [\Delta V_{enc}]&=[C]^T[\Delta V]\\ [R_{active}]&=[C][R_{enc}][C]^T\end{aligned} \quad (4.12)$$

The scalar potential differences caused in the phases winding are attained as:

$$[\Delta V]=[R_{active}][i_{ph}]+j\omega_s[C][P]^T[A] \quad (4.13)$$

Where, $[R_{active}]$ is the resistance of a stator phases winding matrix.

When substituting equation (4.6) in the equation (4.3) then, the voltage equation of the stator windings turns into:

$$\frac{[U]}{j\omega_s}=[R_{ph}][i_{ph}]+[L_{tete}][i_{ph}]+[C][P]^T[A] \quad (4.14)$$

Where, $[R_{ph}]$ is the total resistance of the phases winding matrix:

$$[R_{ph}]=([R_{tete}]+[R_{active}])/\ j\omega_s \quad (4.15)$$

The ends of the rotor are implicit to be equipotential surfaces, so the voltage equations are not established for the rotor winding.

From the above equations, the electromagnetic behavior of the induction motor was obtained by coupling the field and voltage equations of the rotor windings. The nonlinearity due to the saturation of the iron core and the temperature dependency of the electrical conductivity were determined.

V. RESULT AND DISCUSSION

A. Computed results of Iron loss

Evaluation of the iron loss components in every regions of the model permits a deep analysis of distribution of the particular iron losses. The relation of the total iron loss in a specified region above the iron mass correlated to that region is known as particular iron loss. Because of the protected rotor conditions, the iron loss takes place in the rotor [5]. Furthermore, for elementary regions placing on

particular rotor or stator arc, the average iron loss densities were defined as per the following formula,

$$p_k = \frac{1}{mNV_k}\sum_{i=1}^{N} p_i \qquad (5.1)$$

p_k is the average iron loss density related to the k_{th} stator or rotor arc,
m is the specific iron mass, N is the number of elementary regions on the kth arc,
V_k is the elementary iron volume and p_i are the iron losses in the current elementary region.

This method precisely found the without load iron losses in Pulse Width Modulation (PWM) inverter. The measured and computed outcomes of iron losses under PWM supply conditions were shown in the Table 5.1 to 5.5.

Table 5.1.Iron losses in CMI with SF-1300Hz

Switching frequency 1300 Hz, CMI									
$P_{meas}[W]$	457	388	323	250	202	122	91	61	19
$P_{stat}[W]$	286	248	204	162	137	79	59	40	12
$P_{rot}[W]$	194	159	129	100	83	49	37	24	8
$P_{calc}[W]$	480	407	333	262	220	128	96	64	20

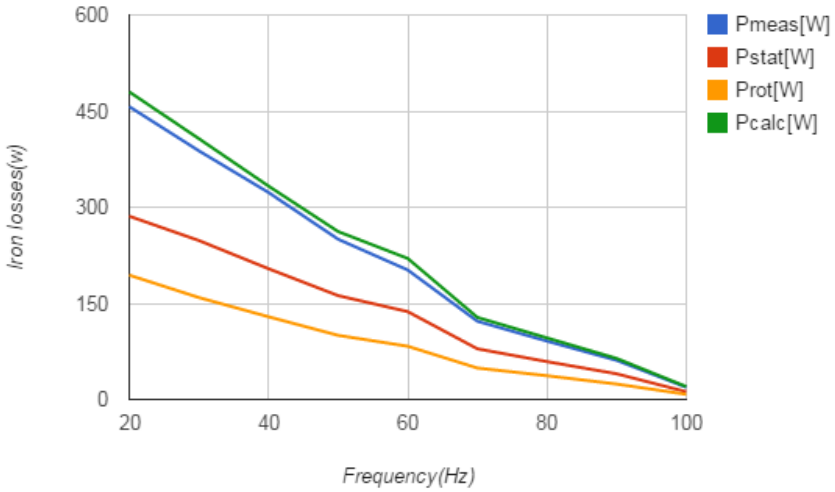

Figure 5.1.Graph of iron losses in CMI with SF-1300Hz

Table 5.2.Iron losses inVMI with SF-1300Hz

Switching frequency 1300 Hz,VMI									
$P_{meas}[W]$	456	413	319	269	218	143	111	82	30
$P_{stat}[W]$	299	266	213	177	142	94	72.5	54	20
$P_{rot}[W]$	184	164	135	108	88	58	43.5	33	12
$P_{calc}[W]$	483	430	348	285	230	152	116	87	32

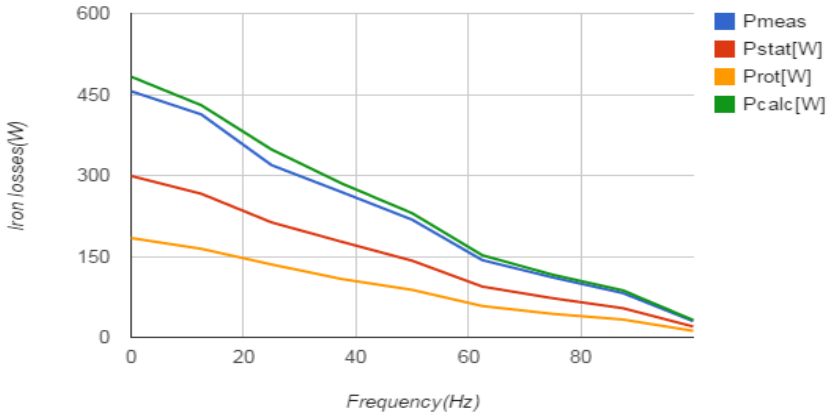

Figure 5.2.Graph of iron losses in VMI with SF-1300Hz

Table 5.3.Iron losses in CMI with SF-2000Hz.

Switching frequency 2000 Hz, CMI									
$P_{meas}[W]$	462	376	318	248	201	122	90	62	20
$P_{stat}[W]$	268	232	203	161	122	74	54	37	13
$P_{rot}[W]$	172	148	128	95	74	46	34	23	7
$P_{calc}[W]$	440	380	331	256	196	120	88	60	20

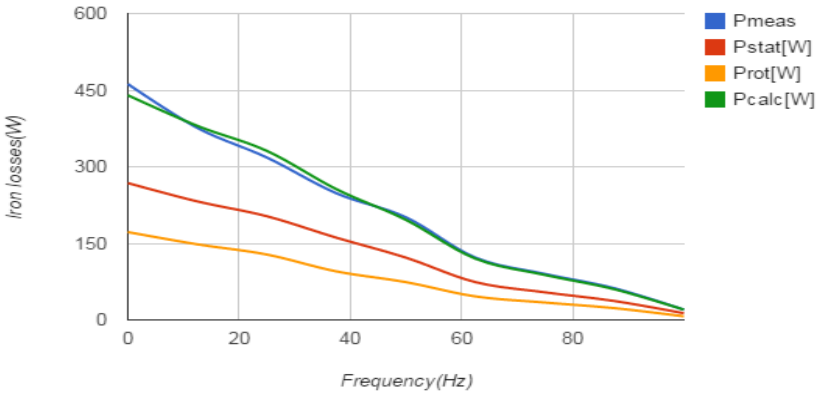

Figure 5.3.Graph of iron losses in CMI with SF-200Hz.

Table 5.4. Iron losses in VMI with SF-2000Hz

Switching frequency 2000 Hz,VMI									
$P_{meas}[W]$	467	390	329	268	223	150	117	88	35
$P_{stat}[W]$	291	244	208	164	126	87	69.4	53.3	20.5
$P_{rot}[W]$	179	150	131	100	77	53	41.6	32.7	12.5
$P_{calc}[W]$	470	394	339	264	203	140	111	86	33

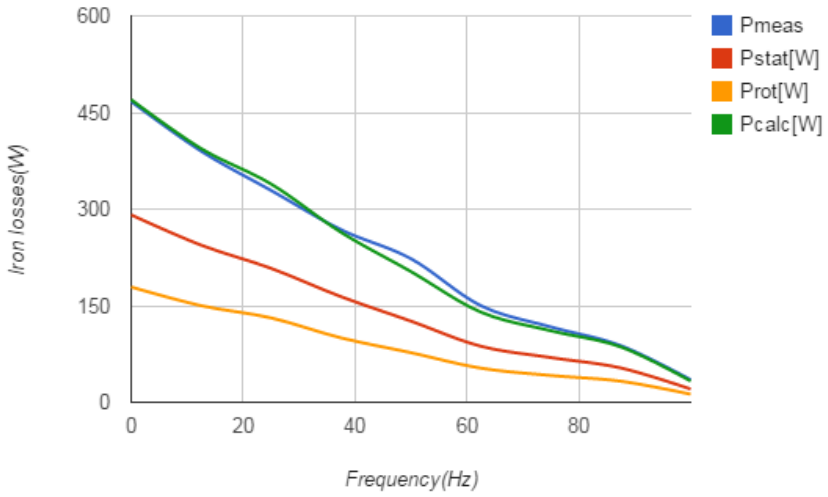

Figure 5.4.Graph of iron losses in VMI with SF-200Hz

Table 5.5.Line-Line voltage with SF -1300 and 2000Hz

Switching frequency 1300Hz		Switching frequency 2000 Hz	
$V_{lin}[V]$		$V_{lin}[V]$	
CMI	VMI	CMI	VMI
229	229	230	230
215	215	215	215
201	200	201	200
180	1802	180	180
160	160	160	160
120	120	120	120
100	100	100	100
80	80	80	80
40	40	40	40

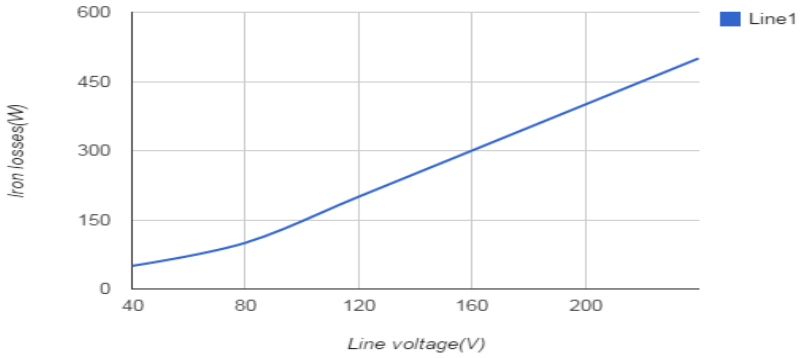

Figure 5.5.Graph of line-line voltage with SF-1300 and 2000Hz

The symbol used in the above Figures and Tables is as follows:

CMI -Constant Modulation Index; VMI - Variable Modulation Index

$P_{meas}[W]$-Measured Iron Losses; $P_{stat}[W]$- Calculated Stator Iron Losses

$P_{rot}[W]$-Calculated Rotor Iron Losses; $P_{calc}[W]$- the Sum of Calculated Iron Losses

$V_{lin}[V]$-Line-to-Line voltage; SF - Switching Frequency.

In the PWM inverter fed induction motors, the outcomes achieved utilizing other methodologies and it is compared with the iron loss prediction error lower than 10% which affirms the integrity of the proposed process.

B. Computation of temperature distribution of rotor under various loads

The lowest temperature bar and the highest temperature bar are chosen for the purpose of study. The bar farther the terminal box has lower temperature and near the terminal box has higher temperature, in which there is no cooling wind at the terminal box. The lowest temperature at the top of the bar in which temperature distribution is in the single bar and progressively decreased from the top to the bottom of the bar. Temperature difference is lower than 0.5°C. The temperature distribution of bar has the highest temperature in the rated load which is shown in Figure 5.6.

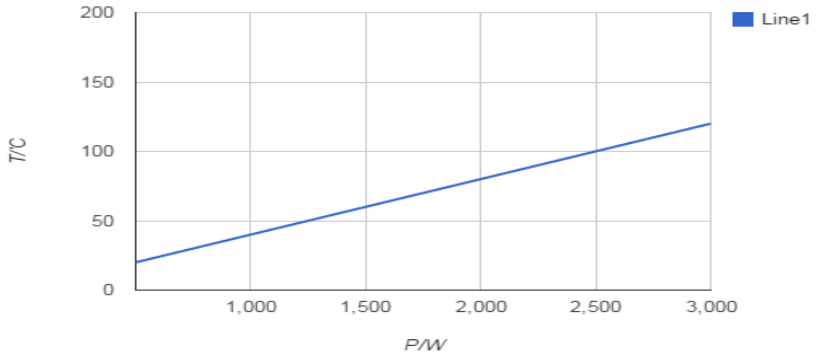

Figure 5.6. Graph of rotor temperature analysis under various load

C. Computation of thermal distribution of rotor under various loads

When the thermal stress in the bar is larger steadily it increases the load. i.e., thermal stress is raise between two types of material in the bar or between slot wall and bar. Discrepancy of the maximum rotor thermal stress with various loads is shown in Figure 5.7. The outcomes demonstrated that when the load increases, the maximum thermal stress is also increases. There is a common extruding between the lower cast aluminum and the upper compound material.

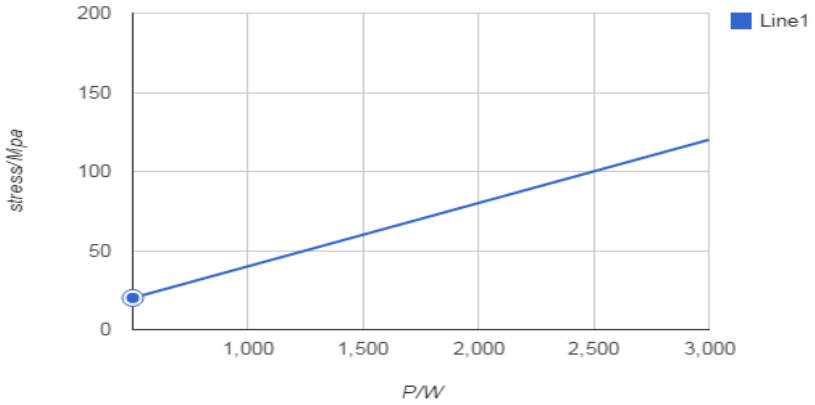

Figure 5.7. Graph of rotor temperature analysis under various load

D. Thermal analysis with FEM

The initial coupling between thermal analysis and AC steady state magnetic, the speed of 1480 rpm is the operating temperature. The thermal time of response is shown in Figure 5.8.
The time of response is in the array of around twenty minutes in this motor.

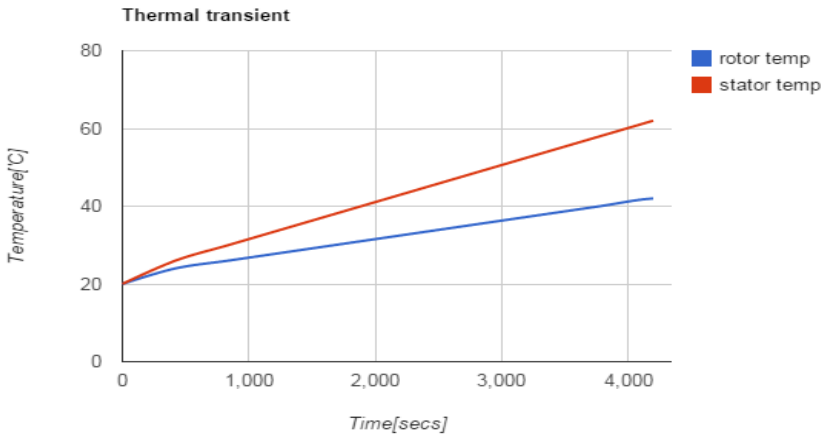

Figure 5.8.Thermal analysis of time response.

Finally, the thermal analysis of induction motor in rotor were computed and determined. The temperature distribution also found and calculated. The switching frequency was used in CMI and VMI to determine the iron losses in rotor and stator.

REFERENCES

[1] Jun-Ci Cao, Rong-Chao Qian and Wei-LI LI.. Calculation and Analysis of 2-D Thermal Stress Field in Induction Motor With Compound Cage Rotor Under Different Load. Applied Mechanics and Materials.Vol.117-119.pp.no.97-100. (2012)

[2] D. C. Franklin and A. Morelato.. Improving Dynamic Aggregation of Induction Motor Models. IEEE Transactions on Power systems.Vol.9.pp.no.1934-1941. (1994)

[3] Jun-Ci Cao, Rong-Chao Qian and Wei-LI LI.. Calculation and Analysis of 2-D Thermal Stress Field in Induction Motor with Compound Cage Rotor Under Different Load. Applied Mechanics and Materials.Vol.117-119.pp.no.97-100. (2012)

[4] Zbigniew Gmyrek, Aldo Boglietti and Andrea Cavagnino.. Estimation of Iron Losses in Induction Motors: Calculation Method, Results, and Analysis. IEEE Transactions On Industrial Electronics.Vol.57.pp.no.161-171. (2010)

[5] M.A.Mueller, S.Williamson, T.J.Flack, K.Atallah, B.Baholo, D.Howe.. Calculation of iron losses from time stepped finite element models of cage induction machine. Proceedings in Interntional Conference in Electric Machines Drives.pp.no.88-92. (1995)

[6] Johan J. C. Gyselinck, Lieven Vandevelde, Dimitre Makaveev and Jan A. A. Melkebeek.. Calculation of No Load Losses in an Induction Motor Using an Inverse Vector Preisach Model and an Eddy Current Loss Model. IEEE Transactions on Magnetics.Vol.36.pp.no.856-860. (2000)

